Photocatalytic Adsorption Synergistic Degradation of Tetracycline by Z-scheme Bi2WO6/ZIF-8

Xiaojun Dai
Changzhou University
sheng feng (shfeng@cczu.edu.cn)
Changzhou University
Wei Wu
Changzhou University
Yun Zhou
Changzhou University
Zhiwei Ye
Changzhou University
Yang Wang
Changzhou University
Xun Cao
Changzhou University

Research Article

Keywords: Bi2WO6/ZIF-8, photocatalysis, degradation of tetracycline, Z-scheme heterojunction

Posted Date: September 11th, 2021

DOI: https://doi.org/10.21203/rs.3.rs-883282/v1

Abstract

In this paper, in order to improved the photocatalytic activity of Bi_2WO_6, Bi_2WO_6 and ZIF-8 were successfully combined by in-situ growth method for the first time. The addition of ZIF-8 effectively inhibited the recombination of photogenerated electron hole pairs and further improved the electron utilization efficiency, and superoxide anion was introduced to greatly improve the photocatalytic activity. The performance of Bi_2WO_6/ZIF-8 in the photodegradation of tetracycline (TC) was studied under different conditions of proportions of ZIF-8, dosage of catalyst and concentration of TC. The results indicated that B/Z/5/1 (10mg) had the best photocatalytic activity, and 97.8% of TC (20mg/L) could be degraded in 80 minutes under UV light, the rate constant (k) for TC degradation was almost 3 times that of Bi_2WO_6. The effects of pH, HA and inorganic anions on the degradation of TC were studied in simulated real water. Further, B/Z/5/1 could be reutilized up to five cycles without reduction of efficiency and catalysis performance. Therefore, Bi_2WO_6/ZIF-8 heterojunction composite material can be utilized as an efficient photocatalyst for remediation of environmental pollution.

Introduction

With the development of society, environmental pollutions, especially the spread of antibiotics in the environment, are becoming more and more serious. One of the most typical is tetracycline. Due to the limited absorption of tetracycline by human body, most of TC flow into the environment and return to human body through various channels, causing drug resistance and threatening human health[1]. The degradation rate of tetracycline in nature is very slow, and the intermediate products are more toxic. The existing process could not completely remove tetracycline[2], so it is urgent to establish the effective degradation methods in the field of environmental protection. Semiconductor photocatalysis technology has unique advantages for pollutant degradation because of its green and high efficiency. Among many semiconductor materials, Bi_2WO_6 is popular because of its high valence band potential energy and easy-to-prepare. As mentioned in the literature review[3], there is a $[WO]^{2-}$ octahedral structure between the $(Bi_2O_2)^{2+}$ layers of Bi_2WO_6, and the electron transfer rate is fast, forming an electric field that can inhibit the recombination of photogenerated electron hole pairs, so the photocatalytic activity is higher than that of general semiconductor materials. However, the specific surface area of Bi_2WO_6 is very small and the photogenerated carriers are unstable[4]. Therefore, how to improve the photocatalytic activity of Bi_2WO_6 is worth studying.

Metal-organic frameworks (MOFs) are a new porous material composed of metal ions and organic ligands[5]. Because of the ordered structure [6], MOFs are good candidates for preparing composite semiconductor materials with large surface area[7]. In the previous report, Bi_2WO_6 and MOFs (such as UiO-66-NH_2) were combined to construct heterojunction, which showed the enhanced dispersion and specific surface area of Bi_2WO_6 and effectively improved the separation and transfer of photogenerated carriers[8]. Compared with Bi_2WO_6, the degradation efficiency of Rhodamine B and Phenol was increased by 1.5 times. Among many MOFs, ZIF-8 has more outstanding performances, such as thermochemical

stability, high porosity and large specific surface area, core-shell g-C_3N_4@ZIF-8 was prepared by in-situ growth of ZIF-8 on g-C_3N_4[9], which has shown that the photocatalytic degradation rate of TC was 4.8 times higher than that of g-C_3N_4. In addition, compared with ZnInS nanosheets, the ZnInS@ZIF-8 composite exhibits higher photocatalytic efficiency, and the photocatalytic degradation efficiency of TC reach 73% in 5 minutes[10]. Hence, the heterojunction of semiconductor materials and MOFs is one of the effective methods[11] to improve the photocatalytic activity and stability of wastewater treatment. Among them, Z-scheme is the most typical, which can extend the range of material response to light, improve the charge transfer efficiency and enhance the photocatalytic activity[12]. However, up to date, there is no report on the construction of Z-scheme heterojunction through combination of Bi_2WO_6 and ZIF-8 that shows the improved photocatalytic degradation efficiency of TC.

In this paper, we prepared a Bi_2WO_6/ZIF-8 Z-scheme with excellent photocatalytic activity by hydrothermal reaction of ZIF-8 with Bi_2WO_6 precursor. It showed strong photocatalytic activity in the degradation of TC by UV light. Through a series of characterization techniques, the morphology and catalytic properties of the composites were studied, and the degradation of TC was further discussed. Finally, the mechanism of photocatalysis was discussed. This research expands the practical application scenarios of MOF materials and may have important significance for the removal of tetracycline or other antibiotics in the future.

Experimental

Preparations of materials

All the reagents used in the experiment were analytical grade and were purchased from Aladdin industrial company, including bismuth pentahydrate ($Bi(NO_3)_3{\cdot}5H_2O$), sodium tungstate Dihydrate ($Na_2WO_4{\cdot}2H_2O$), zinc nitrate hexahydrate ($Zn(NO_3)_2{\cdot}6H_2O$), 2-methylimidozole (2-MeIm), sodium hydroxide (NaOH), methanol (CH_3OH), ethanol (C_2H_5OH), humic acid (HA), ethyl-enediaminetetraacetic acid disodium (EDTA-2Na), tertiary butanol (TBA), p-benzoquinone (BQ), etc. Deionized water was used for all of the experiments. All reagents in this study used without further purification.

Synthesis of materials

Synthesis of ZIF-8

ZIF-8 was prepared according to the literature method[13]. Added $Zn(NO_3)_2 \cdot 6H_2O$ (1 mmol) to 50 mL CH_3OH (A solution), and added 2-MeIm (8 mmol) to 50 mL CH_3OH (B solution). The solution A and B was dissolved by sonication for 30 min. Then slowly drop solution a into solution B and stir vigorously for 6 hours. The solid product was washed and centrifuged with deionized water and CH_3OH, and ZIF-8 was obtained after dried at 60°C for 12 h.

Synthesis of Bi_2WO_6/ZIF-8

Bi_2WO_6/ZIF-8 composite material was synthesized under hydrothermal condition. The mixture of 1 mmol $Bi(NO_3)_3 \cdot 5H_2O$, 0.5 mmol $Na_2WO_4 \cdot 2H_2O$ and 25 mg CTAB was added to a beaker containing 40 mL deionized water[14], and the given mass of ZIF-8 was added in the solution. The mixed reactants was sonicated for 1 h and then stirred for 1 h. After fully mixed, the mixed solution was poured into a 100 ml reactor and was heated at 140°C for 18 h. Then, the product was centrifuged with deionized water and ethanol twice respectively. After centrifugate, the product was dried at 60°C. The compound material with different molar mass ratios (Bi_2WO_6:ZIF-8 = 1:1, 2:1, 5:1 and 7:1) were abbreviated as B/Z/1/1, B/Z/3/1, B/Z/5/1 and B/Z/7/1. Under the above conditions, pure Bi_2WO_6 was prepared as reference.

Characterization

The crystal phases was performed X-ray diffraction (XRD) on D/MAX2500 diffractometer (RIGAKU, Japan). Fourier transform infrared (FTIR) spectra were plotted by using Spectrum One FTIR spectrophotometer (PerkinElmer, USA). The ultraviolet-visible diffuse reflectance spectra (UV-vis DRS) were identified with a Shimadzu UV-2550. The Photoluminescence (PL) spectroscopy of samples were identified with an Edinburgh FL/FS900 spectrophotometer. The binding energy of each element (Bi, W, Zn, C, N and O) was measured by Thermo Scientific K-Alpha. The images of crystal structure was obtained from FEI Talos 200S (TEM) and SUPRA55 (SEM) with energy-dispersive spectroscopy (EDS)..

Photocatalytic experiments

Before the photocatalytic experiments, 20 mg/L TC standard solution was prepared with deionized water. 10 mg catalyst was immersed in 50 mL (20 mg/L) TC solution, which was stirred in dark for 40 min until adsorption equilibrium. Then, the photocatalytic reaction was studied by a 300 W mercury lamp. During this reaction, samples were taken every 20 minutes for spectral analysis. The absorbance of TC at 357 nm was determined by UV-Vis spectrophotometer.

Results And Discussion

Characterizations

The XRD patterns of pure ZIF-8 in Figure. 1a was the same as that reported in literature[5], the diffraction peaks at 2θ = 7.37°, 10.45°, 12.77°, 14.72°, 16.47°, 18.0°, 24.55° were indexed to (011), (002), (112), (022), (013), (222), (233) planes of ZIF-8, respectively. In the Figure 1a, Bi_2WO_6 had five diffraction peaks at 28.3° (113), 32.8° (200), 47.1° (202), 56.0° (133), 58.5° (262), which accurately matched with the Bi_2WO_6 standard card (JCPDS No. 39-0256)[15]. The crystal structure of Bi_2WO_6 was not changed by adding ZIF-8, but the diffraction peak of ZIF-8 was weak compared to those of Bi_2WO_6 and there were no characteristic peaks at low proportions (B/Z), due to uniform dispersion of ZIF-8 and the high crystallinity of Bi_2WO_6. The characteristic peaks of the two monomers could be clearly seen when the proportion was increased to 1/3. These results provided further support that Bi_2WO_6 and ZIF-8 were combined successfully.

The infra-red (FT-IR) spectrum of the prepared sample was shown in Figure. 1b. The peaks at 3448 cm^{-1}, 3136 cm^{-1} and 2930 cm^{-1} were assigned to the stretching vibration of N-H bond, imidazole aromatics and C-H bond in the imidazole ring of ZIF-8. The in-plane bending of pyridine ring forms several peaks in the range of 902 ~ 1306 cm^{-1}. The peak near 421 cm^{-1} was assigned to the stretching vibration of Zn-N bond[16]. The absorption band at 1384 cm^{-1}, 729 cm^{-1} and 580 cm^{-1} were very strong, which may be caused by Bi-O, W-O and W-O-W stretching[15]. The peak at 1629 cm^{-1} were attributed to O-H bending of absorbed water moleculesmay. The corresponding peak could also be seen in the composite[17]. It is evident that the functional groups of the two monomers were retained in the composites.

The photoelectron-hole (E-H) recombination rate of the composite was analyzed by PL spectroscopy. The higher the PL peak strength, the lower the separation efficiency of E-H[13]. It could be seen from Figure.1c that the peak intensity of pure ZIF-8 was the strongest, and it showed that the recombination rate of E-H was very fast. The peak intensity of the composites was lower than that of Bi_2WO_6, which indicates that the separation rate of photoexcited interface charge of the composite was improved[18], and it also confirmed that the recombination of Bi_2WO_6 and ZIF-8 inhibits the recombination efficiency of photogenerated electron hole pairs, thus enhancing the photocatalytic activity. And the E-H recombination rate of B/Z/5/1 was the lowest.

The structure of the composite was studied by scanning electron microscope and transmission electron microscope. In Figure. 3a, ZIF-8 presented regular dodecahedron structure, which was consistent with that reported in the literature[19]. The Bi_2WO_6 in Figure 3b showed nano flakes with the size of 50-200 nm[20]. Figure. 3C was the SEM image of B/Z/5/1. It could be seen that Bi_2WO_6 was tightly loaded on the surface of ZIF-8, which was further confirmed by high power transmission electron microscopy (Figure. 3d and 3e). The successful combination of the two materials could also be confirmed by EDS. From Figure. g, the chemical composition of both ZIF-8 and Bi_2WO_6 could be clearly seen, including C, O, W, Bi and Zn. High power TEM photographs of B/Z/5/1 showed that the structure and lattice fringes of the sample were very clear, and the measured lattice spacing was 0.315 nm[15], which matched with the crystal plane (131) of Bi_2WO_6[21]. B/Z/5/1 is expected to effectively inhibit the rapid recombination of carriers and improve the photocatalytic activity due to the close contact between Bi_2WO_6 and ZIF-8. Hence, the above analysis could prove that the preparation of Bi_2WO_6 and ZIF-8 composite were successfully.

The chemical composition and bonding configuration of B/Z/5/1 were determined by X-ray photoelectron spectroscopy (XPS). Figure. 4a was full spectrum XPS scan of B/Z/5/1 and Bi_2WO_6, the elements, including Bi, W, Zn, C and O, could be clearly seen, and due to the recombination of ZIF-8, the main peaks of Bi and W elements were weakened. Figure. 4b presented the high-resolution XPS spectrum of Bi 4f. The two peaks at 158.48 eV and 163.68 eV correspond to the photoelectron responses of Bi $4f_{7/2}$ and Bi $4f_{5/2}$ in Bi_2WO_6[22], and it proved that there was a combination of Bi of trivalence state in Bi_2WO_6[23]. Figure. 4c presented the high-resolution XPS spectrum of W. The two peaks at 35.05 eV and 37.17 eV correspond to the photoelectron responses of W $4f_{7/2}$ and W $fp_{5/2}$ in Bi_2WO_6, which is indicative of the

existence of W^{6+} in Bi_2WO_6[24]. In Figure. 4d, the peaks of 1021.6 eV (Zn $2p_{3/2}$) and 1044.8 eV (Zn $2p_{1/2}$) were caused by ZIF-8[6], the peak of B/Z/5/1 near the binding energy of 1027.6 eV was very weak. In Figure. 4f, two dominant peaks at 284.3 eV and 285.2 eV correspond to C=C and N=C-N bonds, respectively[25]. The results of XPS indicated that Bi_2WO_6 and ZIF-8 coexist in the composites.

Analysis of the photocatalytic reactions

Adsorption experiments

Due to the strong adsorption properties of the two monomers, a separate study on the adsorption properties of the materials was undertaken. Before studying the photocatalytic performance of the material, the adsorption studies of samples were performed in the dark to determine the reaction time when the material reached the adsorption equilibrium.10 mg of catalyst was added into 25 mg/L TC solution and the dark reaction time was prolonged to 1 hour. As shown in Figure. 5a, the adsorption efficiency of Bi_2WO_6 for TC was only 6%, and that of ZIF-8 for TC was as high as 50%. The adsorption properties of the composites were improved, and increased with the increasing proportion of ZIF-8. It could be seen from Figure. 5a that the adsorption of TC on all materials tends to be stable in about 40 minutes, and it could be determined that the adsorption equilibrium was reached.

Photocatalytic degradation of TC

20 mg/L TC solution was used as the target, and 10 mg of catalytic material was added respectively. First, 40 minute dark reaction was carried out to complete the adsorption process of the material. As shown in Figure. 5b, in the absence of catalyst, TC hardly degraded after 80 minutes of UV irradiation. Compared with the two monomers, the photocatalytic performance of the composites was improved, especially for B/Z/5/1. After adsorption for 40 min and UV irradiation for 80 min, the degradation efficiency of TC reached 97.8%. One of the reasons should be ascribed to the improved specific surface area and surface active sites[26]. Another reason was that the heterojunction formed in the composite could change electron transfer routes and improve electron utilization efficiency, which thus improves the photocatalytic activity[12,27,28].

As shown in Figure. 5c and 6d, the kinetics of TC degradation and the calculated rate constant were match with the experimental degradation results. It was confirmed that the degradation efficiency of B/Z/5/1 was the best. The effect of different catalytic dosage on the degradation of TC was within the scope of assumption. The excessive catalyst dosage did not help the degradation of TC too much. The dosage of 10 mg was the most suitable. The degradation efficiency of different TC concentration was different. When TC concentration was 10 mg/L, the degradation rate was the most rapid. When TC concentration was 100 mg/L, the degradation rate was the lowest, which indicates the absorption of UV light by TC would affect the absorption of the material.

Cyclic experiments

Cyclic experiment was the main way to evaluate the stability of materials. After each photocatalytic experiment, the material was centrifuged, dried and recycled. This process was repeated five times and the photocatalytic efficiency of each experiment was recorded. As shown in Figure 6, after five cycles of experiments, the photocatalytic activity of B/Z/5/1 was still very high (88.7%). The XRD patterns of the fifth experiment and the first experiment have no obvious change. The results suggested that the crystal structure of the composite is highly stable and shows no obvious change during the photocatalytic process[29].

Analysis of photocatalytic degradation of TC

The optical absorption characteristics of the three materials was analyzed by UV-Vis absorption spectra. In Figure. 7a, the absorption edge of Bi_2WO_6 was 468 nm, and the result was consistent with the literature[30,31]. The absorption edge of ZIF-8 was about 250 nm and it had no response to visible light[32]. Due to the composition of Bi_2WO_6 and ZIF-8, the absorption edge of the composite were decreased. With the increased of the specific gravity of ZIF-8, the absorption boundary of the composite decreased gradually. The absorption boundary of B/Z/1/1 was decreased to 447 nm.

The intersection of the tangent and the X-axis in Figure. 7b could be considered as an approximation of the band-gap energy. The band gap of ZIF-8 and Bi_2WO_6 were 4.8 eV and 2.89 eV, respectively, which were consistent with the literature[33,34]. With the increased of ZIF-8, the band gap of the composite became wider. The band gap of B/Z/1/1 was increased to 3.22 eV. which was consistent with the expectation.

The band-gap energies of ZIF-8, Bi_2WO_6, B/Z/1/1, B/Z/3/1, B/Z/5/1 and B/Z/7/1 could be calculated by equation (1).

$$(ahv)=A(hv-Eg)^{1/n} \quad (1)$$

The VB and CB could be calculated by equation (1) and (1)

$$E_{VB}=X-E^{e}+0.5E_{g} \quad (2)$$

$$E_{CB}=E_{VB}+E_{g} \quad (3)$$

In formula, *a*, *h*, *A* and *v* refer to absorption coefficient, Planck constant, proportion constant and optical frequency, respectively. If the material has direct band gap, then n was 2. Conversely, if the material has indirect band gap, then n was 1/2[35].

Photoelectrochemical analysis

The separation and transfer of charge carriers was studied by electrochemical characterization of the materials. As shown in Figure. 8a, the transient photocurrent density of B/Z/5/1 was much higher than that of ZIF-8 and Bi_2WO_6, which showed that the combination of ZIF-8 and Bi_2WO_6 improved the separation of photo-excited carriers and photocatalytic performance[36]. It was consistent with the results of PL.

The charge separation effect of the material was studied by electrochemical impedance spectroscopy (EIS). The Nyquist curve in Figure. 8b showed that the arc radius of the composite was significantly smaller than that of ZIF-8 and Bi_2WO_6. The radius on the Nyquist curve representd the separation and transfer velocity of optically excited electron hole pairs. The smaller the radius, the faster the separation and transfer velocity[37]. Therefore, the addition of ZIF-8 was beneficial to inhibit charge recombination.

Simulating real water quality

Water quality in nature is very complex, which will affect the degradation of TC. By adjusting the pH value, added HA and anions, the change of degradation efficiency of B/Z/5/1 in simulated water quality was explored. The pH value had great influence on the photocatalytic degradation, therefore, the pH value of photocatalytic water matrix was adjusted, and the degradation efficiency of TC by B/Z/5/1 at different pH values was studied. As shown in Figure. 9, the degradation of TC by B/Z/5/1 was highly pH dependent. Under acidic conditions, the degradation efficiency of TC by B/Z/5/1 was inhibited with the decreasing pH. The absorbance intensity of TC was affected by pH value, the lower the pH value, the weak the absorbance. Therefore, the extinction efficiency decreased with the decreasing pH[38]. In addition, the dissociation morphology of TC changed at different pH values. With the increasing pH, TC gradually transformed into ions that were easy to be degraded due to deprotonation reaction[39]. Therefore, under alkaline conditions, the adsorption performance and photocatalytic efficiency of the material for TC were greatly improved. HA could reduce the degradation efficiency of TC, which may be induced by the reaction of HA with ·OH in aqueous solution. The capture experiment demonstrated that the key factor of TC degradation was ·OH[40]. Secondly, HA could absorb ultraviolet light in aqueous solution, which was fatal in UV photocatalytic degradation system[41]. HCO_3^- was helpful to the degradation of TC. Because under neutral conditions, HCO_3^- would generate CO_3^{2-}·[42]. Cl^- also reduced photocatalytic efficiency because Cl^- would react with ·OH during photocatalysis[43].

Free radical capture experiment

In exploring the mechanism of photocatalysis, different corresponding active substances were added to capture hydroxyl radicals, holes and superoxide anions to study the photocatalytic reaction process[39-41]. As shown in Figure. 10, in presence of BQ and TBA, the adsorption performance and photocatalytic efficiency of the material for TC decreased significantly. The presence of EDTA-2Na had little effect on the

reaction. The results of capture experiments confirmed that superoxide anion and hydroxyl radical were crucial in the degradation of TC.

Photocatalytic mechanism

The mechanism of photocatalytic reaction was analyzed by characterization and experimental results. The band gap of Bi_2WO_6 and ZIF-8 was 2.89 eV and 4.8 eV, respectively, by UV-visible diffuse reflectance. By further calculation, the E_{CB} and E_{VB} of Bi_2WO_6 were 0.49 eV and 3.38 eV, and those of ZIF-8 were -3.26 eV and 1.52 eV. The mechanism of photocatalysis was understood by the transfer path of photogenerated electrons and holes. Under UV irradiation, the electrons of Bi_2WO_6 and ZIF-8 migrated from VB to CB, and the electron transfer path was Z-type. Because the CB (0.117 eV) of Bi_2WO_6 was larger than $O_2/\cdot O_2^-$ (-0.35 eV), it was difficult for the photogenerated electrons of CB to form $\cdot O_2^-$ with O_2. Finally, the photoinduced electrons on the CB of Bi_2WO_6 could only be transferred to the VB of ZIF-8, and compound with the hole of ZIF-8. Thus, the recombination of electron hole pairs in ZIF-8 was effectively inhibited. Most of the electrons on the CB of ZIF-8 degraded TC by reducing oxygen to form superoxide anion. Secondly, due to the VB potential of Bi_2WO_6 (3.38 eV) was higher than the oxidation potential of water (2.4 eV)[44]. Therefore, some of the holes degraded TC by oxidizing water to hydroxyl groups. The capture experiments indicated that hydroxyl radicals played a more important role than holes in the whole photocatalytic process, so it could be inferred that most of the holes generated on the VB of Bi_2WO_6 reacted with water to form hydroxyl radicals. Thus, TC was effectively degraded. According to these data, it could infer that superoxide anion and hydroxyl radical were crucial in the whole photocatalytic process. This was consistent with the experimental results. The conclusion obtained by analyzing the photocatalytic process matched with the photocatalytic mechanism of Z-scheme[12]. The composite of Bi_2WO_6 and ZIF-8 could effectively inhibit the recombination of photogenerated electron-hole pairs, thus enhanced the photocatalytic activity. The possible process was displayed in formulas (4)-(8).

$$Bi_2WO_6/ZIF\text{-}8 + hv = Bi_2WO_6/ZIF\text{-}8(e^-) + Bi_2WO_6/ZIF\text{-}8(h^+) \quad (4)$$

$$Bi_2WO_6/ZIF\text{-}8(h^+) + H_2O = Bi_2WO_6/ZIF\text{-}8 + OH^- + H^+ \quad (5)$$

$$Bi_2WO_6/ZIF\text{-}8(h^+) + OH^- = Bi_2WO_6/ZIF\text{-}8 + \cdot OH \quad (6)$$

$$Bi_2WO_6/ZIF\text{-}8(e^-) + O_2 = Bi_2WO_6/ZIF\text{-}8 + \cdot O_2^- \quad (7)$$

$$Bi_2WO_6/ZIF\text{-}8(h^+)/\cdot OH/\cdot O_2^- + TC = CO_2 + H_2O + \cdots \quad (8)$$

Conclusion

In summary, the composite of Bi_2WO_6 and ZIF-8 was successfully prepared, which promoted the degradation of TC. Transient photocurrent response and EIS revealed the photoelectrochemical properties

of B/Z/5/1, the addition of ZIF-8 could effectively inhibit the recombination of electron and hole, increase the utilization efficiency of light, and greatly improve the photocatalytic activity. The conduction band potential of ZIF-8 was lower than the redox potential of oxygen. The $\cdot O_2^-$ produced by ZIF-8 was the main factor to improved the photocatalytic activity. At the same time, the strong adsorption performance of ZIF-8 attracted TC molecules to contacted with active substances. Among composites of different proportions, B/Z/5/1 had the optimal catalytic activity and high cycle stability, which was consistent with the Z-type photocatalytic mechanism. In addition, the photocatalytic degradation for the composite with B/Z/5/1 was highly dependent on pH value, and the degradation efficiency was the maximum under Neutral pH conditions, and B/Z/5/1 still had a good degradation efficiency of TC in simulated real water. Finally, this work showed that ZIF-8 can enhance the efficiency of Bi_2WO_6 photocatalytic degradation of TC, and as an excellent photocatalytic composite, it is expected to provide an important reference for future research.

Declarations

CRediT authorship contribution statement

Xiaojun Dai: Subject idea, subject experimental design, subject data acquisition, article writing. **Sheng Feng**: Solve relevant academic problems and optimize relevant experiments. **Wei Wu**: Optimize icon details. **Yun Zhou, Zhiwei Ye**, **Yang Wang**, **Xun Cao**: Related auxiliary work.

Acknowledgements

The author sincerely thanks the National Natural Science Foundation of China (No.22075032) and the Jiangsu Graduate Research and Practice Innovation Program (KYCX21_2876, SJCX21_1196) for funding.

Declaration of interest statement

All the authors of this article declare that there is no dispute over economic interests with the work entitled “Photocatalytic adsorption synergistic degradation of tetracycline by Z-scheme Bi2WO6/ZIF-8”.

References

[1] Hu, K., et al., Ternary Z-scheme heterojunction of Bi2WO6 with reduced graphene oxide (rGO) and meso-tetra (4-carboxyphenyl) porphyrin (TCPP) for enhanced visible-light photocatalysis. Journal of Colloid and Interface Science, 2019. **540**: p. 115-125, https://doi.org/10.1016/j.jcis.2019.01.013.

[2] Afreen, G., M. Shoeb, and S. Upadhyayula, Effectiveness of reactive oxygen species generated from rGO/CdS QD heterostructure for photodegradation and disinfection of pollutants in waste water.

Materials Science and Engineering: C, 2020. 108: p. 110372, https://doi.org/10.1016/j.msec.2019.110372.

[3] Lv, Y., et al., Fabrication of Wide–Range–Visible Photocatalyst Bi2WO6–x nanoplates via Surface Oxygen Vacancies. Scientific Reports, 2016. **6**(1): p. 19347, https://doi.org/10.1038/srep19347.

[4] Miao, B., et al., Sb2WO6/Bi2WO6 composite photocatalyst prepared by one-step hydrothermal method: Simple synthesis and excellent visible-light photocatalytic performance. Materials Science in Semiconductor Processing, 2021. **125**: p. 105636, https://doi.org/10.1016/j.mssp.2020.105636.

[5] Jiang, M., et al., Hierarchically Porous N-doped Carbon Derived from ZIF-8 Nanocomposites for Electrochemical Applications. Electrochimica Acta, 2016. **196**: p. 699-707, https://doi.org/10.1016/j.electacta.2016.02.094.

[6] Qiu, M., et al., The photocatalytic reduction of U(VI) into U(IV) by ZIF-8/g-C3N4 composites at visible light. Environmental Research, 2021. **196**: p. 110349, https://doi.org/10.1016/j.envres.2020.110349.

[7] Malik, A. and M. Nath, Multicore–shell nanocomposite formed by encapsulation of WO3 in zeolitic imidazolate framework (ZIF-8): As an efficient photocatalyst. Journal of Environmental Chemical Engineering, 2019. 7(5): p. 103401, https://doi.org/10.1016/j.jece.2019.103401.

[8] Li, G., et al., In-situ growth UiO-66-NH2 on the Bi2WO6 to fabrication Z-scheme heterojunction with enhanced visible-light driven photocatalytic degradation performance. Colloids and Surfaces A: Physicochemical and Engineering Aspects, 2020. **603**: p. 125256, https://doi.org/10.1016/j.colsurfa.2020.125256.

[9] Yuan, X., et al., Design of core-shelled g-C3N4@ZIF-8 photocatalyst with enhanced tetracycline adsorption for boosting photocatalytic degradation. Chemical Engineering Journal, 2021. **416**: p. 129148, https://doi.org/10.1016/j.cej.2021.129148.

[10] Gao, Y., et al., Design and in situ synthesis of ZnInS@ZIF-8-nanofilms multifunctional nanocomposite: A case application for simultaneous fluorescent sensing and enhanced photocatalytic performance toward antibiotic. Microporous and Mesoporous Materials, 2021. **315**: p. 110916, https://doi.org/10.1016/j.micromeso.2021.110916.

[11] Chang, N., et al., Facile construction of Z-scheme AgCl/Ag-doped-ZIF-8 heterojunction with narrow band gaps for efficient visible-light photocatalysis. Colloids and Surfaces A: Physicochemical and Engineering Aspects, 2021. **616**: p. 126351, https://doi.org/10.1016/j.colsurfa.2021.126351.

[12] Lai, Y.-J. and D.-J. Lee, Pollutant degradation with mediator Z-scheme heterojunction photocatalyst in water: A review. Chemosphere, 2021. 282: p. 131059, https://doi.org/10.1016/j.chemosphere.2021.131059.

[13] Yurtsever, H.A. and A.E. Çetin, Fabrication of ZIF-8 decorated copper doped TiO2 nanocomposite at low ZIF-8 loading for solar energy applications. Colloids and Surfaces A: Physicochemical and Engineering Aspects, 2021. 625: p. 126980, https://doi.org/10.1016/j.colsurfa.2021.126980.

[14] Chankhanittha, T., et al., Preparation, characterization, and photocatalytic study of solvothermally grown CTAB-capped Bi2WO6 photocatalyst toward photodegradation of Rhodamine B dye. Optical Materials, 2021. 117: p. 111183, https://doi.org/10.1016/j.optmat.2021.111183.

[15] Zhang, X., et al., Preparation and mechanism investigation of Bi2WO6/UiO-66-NH2 Z-scheme heterojunction with enhanced visible light catalytic activity. Inorganic Chemistry Communications, 2020. **120**: p. 108162, https://doi.org/10.1016/j.inoche.2020.108162.

[16] Ordoñez, M.J.C., et al., Molecular sieving realized with ZIF-8/Matrimid® mixed-matrix membranes. Journal of Membrane Science, 2010. **361**(1): p. 28-37, https://doi.org/10.1016/j.memsci.2010.06.017.

[17] He, Y., et al., Photocatalytic degradation of tetracycline by metal-organic frameworks modified with Bi2WO6 nanosheet under direct sunlight. Chemosphere, 2021. 284: p. 131386, https://doi.org/10.1016/j.chemosphere.2021.131386.

[18] Zhang, Y., et al., Nanocomposite of Ag–AgBr–TiO2 as a photoactive and durable catalyst for degradation of volatile organic compounds in the gas phase. Applied Catalysis B: Environmental, 2011. 106(3): p. 445-452, https://doi.org/10.1016/j.apcatb.2011.06.002.

[19] Dai, H., et al., Recent advances on ZIF-8 composites for adsorption and photocatalytic wastewater pollutant removal: Fabrication, applications and perspective. Coordination Chemistry Reviews, 2021. **441**: p. 213985, https://doi.org/10.1016/j.ccr.2021.213985.

[20] Chankhanittha, T., et al., Enhanced photocatalytic performance of ZnO/Bi2WO6 heterojunctions toward photodegradation of fluoroquinolone-based antibiotics in wastewater. Journal of Physics and Chemistry of Solids, 2021. **153**: p. 109995, https://doi.org/10.1016/j.jpcs.2021.109995.

[21] Meng, X., H. Qin, and Z. Zhang, New insight into the enhanced visible light-driven photocatalytic activity of Pd/PdCl2-doped Bi2WO6 photocatalysts. Journal of Colloid and Interface Science, 2018. **513**: p. 877-890, https://doi.org/10.1016/j.jcis.2017.12.009.

[22] Arif, M., et al., Layer-assembled 3D Bi2WO6 hierarchical architectures by Ti-doping for enhanced visible-light driven photocatalytic and photoelectrochemical performance. Journal of Alloys and Compounds, 2019. **792**: p. 878-893, https://doi.org/10.1016/j.jallcom.2019.03.321.

[23] Wang, G. and L. Wang, Hydrothermal synthesis of rose-like AgVO3/Bi2WO6 heterojunctions with enhanced visible-light-driven photocatalytic activity. Physica E: Low-dimensional Systems and Nanostructures, 2018. **103**: p. 323-328, https://doi.org/10.1016/j.physe.2018.06.021.

[24] Bing, X., et al., Biomimetic synthesis of Bi2O3/Bi2WO6/MgAl-CLDH hybrids from lotus pollen and their enhanced adsorption and photocatalysis performance. Journal of Photochemistry and Photobiology A: Chemistry, 2018. **364**: p. 449-460, https://doi.org/10.1016/j.jphotochem.2018.06.030.

[25] Zhu, W., et al., Microwave-assisted synthesis of Ag-doped MOFs-like organotitanium polymer with high activity in visible-light driven photocatalytic NO oxidization. Applied Catalysis B: Environmental, 2015. **172-173**: p. 46-51, https://doi.org/10.1016/j.apcatb.2015.02.003.

[26] Yang, X., et al., In situ preparation of porous metal-organic frameworks ZIF-8@Ag on poly-ether-ether-ketone with synergistic antibacterial activity. Colloids and Surfaces B: Biointerfaces, 2021. **205**: p. 111920, https://doi.org/10.1016/j.colsurfb.2021.111920.

[27] Yan, S., et al., Z-scheme interface modification by MnV2O6 for V2O5/g-C3N4 heterostructure towards efficient visible photocatalytic activity. Journal of Alloys and Compounds, 2021. **882**: p. 160751, https://doi.org/10.1016/j.jallcom.2021.160751.

[28] Ni, J., et al., Hierarchical defect-rich flower-like BiOBr/Ag nanoparticles/ultrathin g-C3N4 with transfer channels plasmonic Z-scheme heterojunction photocatalyst for accelerated visible-light-driven photothermal-photocatalytic oxytetracycline degradation. Chemical Engineering Journal, 2021. **419**: p. 129969, https://doi.org/10.1016/j.cej.2021.129969.

[29] Chen, F., et al., Highly efficient removal of bisphenol A by a three-dimensional graphene hydrogel-AgBr@rGO exhibiting adsorption/photocatalysis synergy. Applied Catalysis B: Environmental, 2017. **217**: p. 65-80, https://doi.org/10.1016/j.apcatb.2017.05.078.

[30] Lei, S., et al., Enhanced photocatalytic activity of N134 carbon black modified Bi2WO6 benefited from ample oxygen vacancies and boosted separation of photoexcited carriers. Materials Research Bulletin, 2021. **133**: p. 111075, https://doi.org/10.1016/j.materresbull.2020.111075.

[31] Wang, R., et al., A spherical TiO2-Bi2WO6 composite photocatalyst for visible-light photocatalytic degradation of ethylene. Colloids and Surfaces A: Physicochemical and Engineering Aspects, 2020. **602**: p. 125048, https://doi.org/10.1016/j.colsurfa.2020.125048.

[32] Razavian, M., et al., Nickel supported ZIF-8.PEG modified catalyst: A designed active catalyst with high H2 productivity in steam reforming of ethanol at moderate temperature. Journal of Environmental Chemical Engineering, 2021. **9**(4): p. 105531, https://doi.org/10.1016/j.jece.2021.105531.

[33] Zhang, Y. and S.-J. Park, Facile construction of MoO3@ZIF-8 core-shell nanorods for efficient photoreduction of aqueous Cr (VI). Applied Catalysis B: Environmental, 2019. **240**: p. 92-101, https://doi.org/10.1016/j.apcatb.2018.08.077.

[34] Huang, Y., et al., In-situ construction of WC/Bi2WO6 nanocomposites for efficient photodegradation of bisphenol A with peroxymonosulfate activation. Ceramics International, 2021.

47(14): p. 20626-20637, https://doi.org/10.1016/j.ceramint.2021.04.072.

[35] Ni, J., et al., Hierarchical defect-rich flower-like BiOBr/Ag nanoparticles/ultrathin g-C3N4 with transfer channels plasmonic Z-scheme heterojunction photocatalyst for accelerated visible-light-driven photothermal-photocatalytic oxytetracycline degradation. Chemical Engineering Journal, 2021. 419: p. 129969, https://doi.org/10.1016/j.cej.2021.129969.

[36] Liang, Q., et al., Fabrication of BiOI@UIO-66(NH2)@g-C3N4 ternary Z-scheme heterojunction with enhanced visible-light photocatalytic activity. Applied Surface Science, 2018. 456: p. 899-907, https://doi.org/10.1016/j.apsusc.2018.06.173.

[37] Z.Y. Liang, C.X. Zhou, J. Yang, Q.F. Mo, Y.M. Zhang, Y. Tang, Visible light responsive Bi2WO6/BiOCl heterojunction with enhanced photocatalytic activity for degradation of tetracycline and rhodamine B, Inorg. Chem. Commun. 93 (2018) 136–139, https://doi.org/10.1016/j.inoche.2018.05.022.

[38] Golshan, M., et al., Photocatalytic activation of peroxymonosulfate by TiO2 anchored on cupper ferrite (TiO2@CuFe2O4) into 2,4-D degradation: Process feasibility, mechanism and pathway. Journal of Hazardous Materials, 2018. **359**: p. 325-337, https://doi.org/10.1016/j.jhazmat.2018.06.069.

[39] Xu, M., et al., Comparison of UVC and UVC/persulfate processes for tetracycline removal in water. Chemical Engineering Journal, 2020. 384: p. 123320, https://doi.org/10.1016/j.cej.2019.123320.

[40] Gao, X., et al., Enhanced photocatalytic performance of BiOCl for carbamazepine degradation by coupling H-ZSM-5 and modifying phosphate groups: Improved charge separation efficiency with high redox ability. Journal of the Taiwan Institute of Chemical Engineers, 2019. **104**: p. 301-309, https://doi.org/10.1016/j.jtice.2019.08.022.

[41] Arghavan, F.S., et al., Complete degradation of tamoxifen using FeNi3@SiO2@ZnO as a photocatalyst with UV light irradiation: A study on the degradation process and sensitivity analysis using ANN tool. Materials Science in Semiconductor Processing, 2021. **128**: p. 105725, https://doi.org/10.1016/j.mssp.2021.105725.

[42] Liu, Y., et al., Significant role of UV and carbonate radical on the degradation of oxytetracycline in UV-AOPs: Kinetics and mechanism. Water Research, 2016. **95**: p. 195-204, https://doi.org/10.1016/j.watres.2016.03.011.

[43] Ji, Y., et al., Thermo-activated persulfate oxidation system for tetracycline antibiotics degradation in aqueous solution. Chemical Engineering Journal, 2016. **298**: p. 225-233, https://doi.org/10.1016/j.cej.2016.04.028.

[44] Zhang, Q., et al., Solvothermal synthesis of Z-scheme AgIn5S8/Bi2WO6 nano-heterojunction with excellent performance for photocatalytic degradation and Cr(VI) reduction. Journal of Alloys and Compounds, 2019. **805**: p. 41-49, https://doi.org/10.1016/j.jallcom.2019.06.331.

Figures

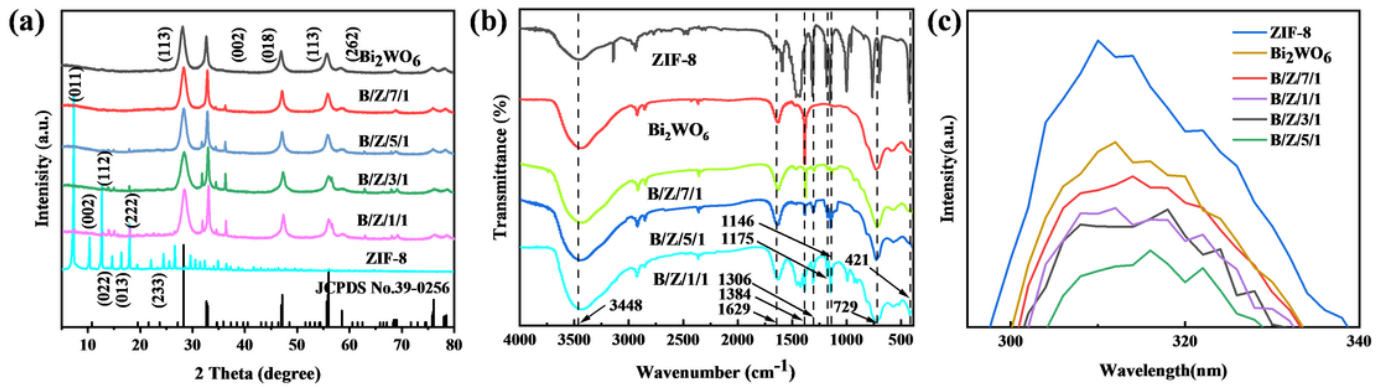

Figure 1

XRD patterns (a), FTIR spectra (b) and Photoluminescence (PL) spectra (c) of samples.

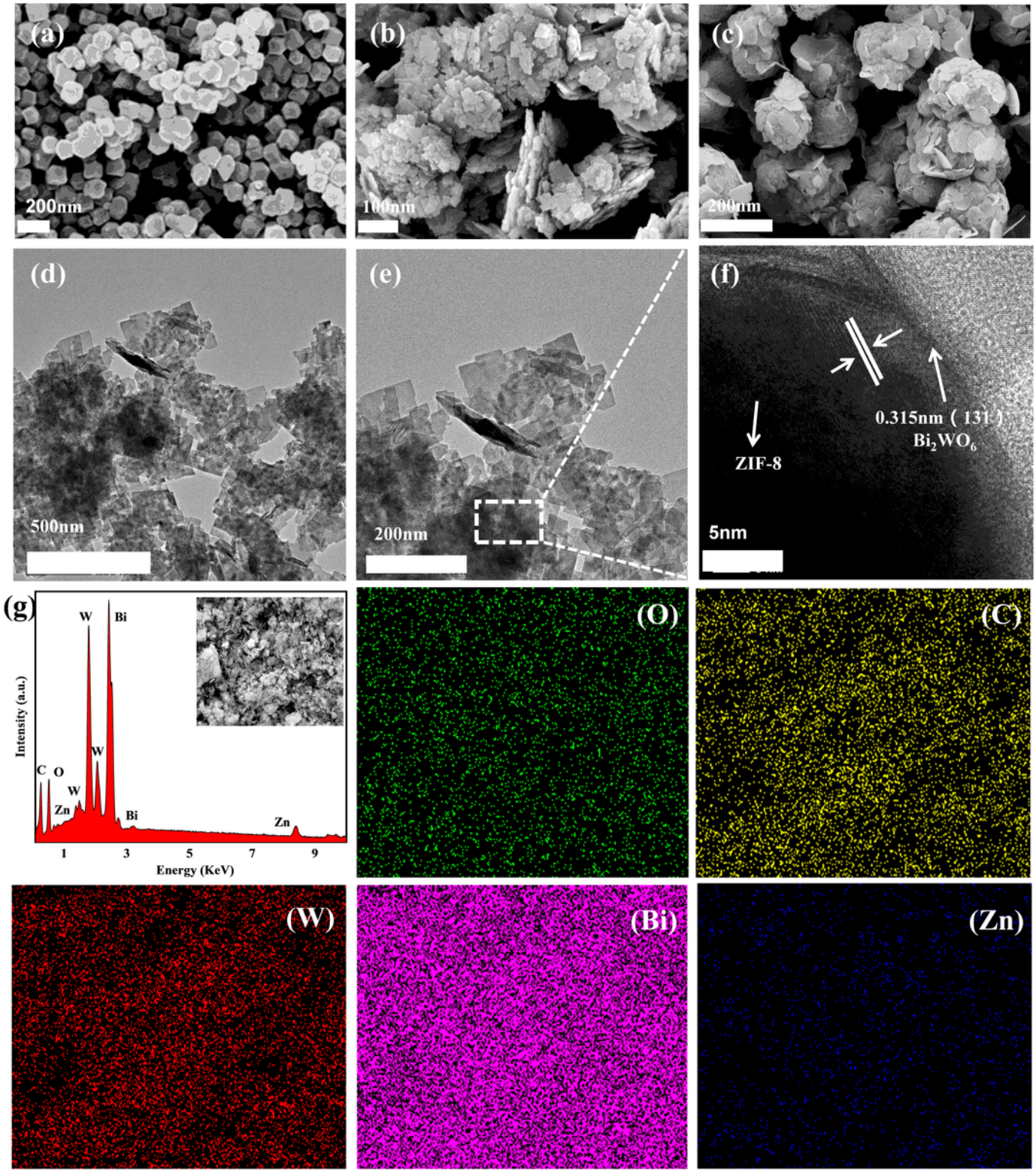

Figure 2

SEM images of ZIF-8 (a), Bi2WO6 (b), B/Z/5/1 (c); TEM image of B/Z/5/1 heterostructures (d, e, f); FESEM-EDS pattern and mapping of B/Z/5/1 (g).

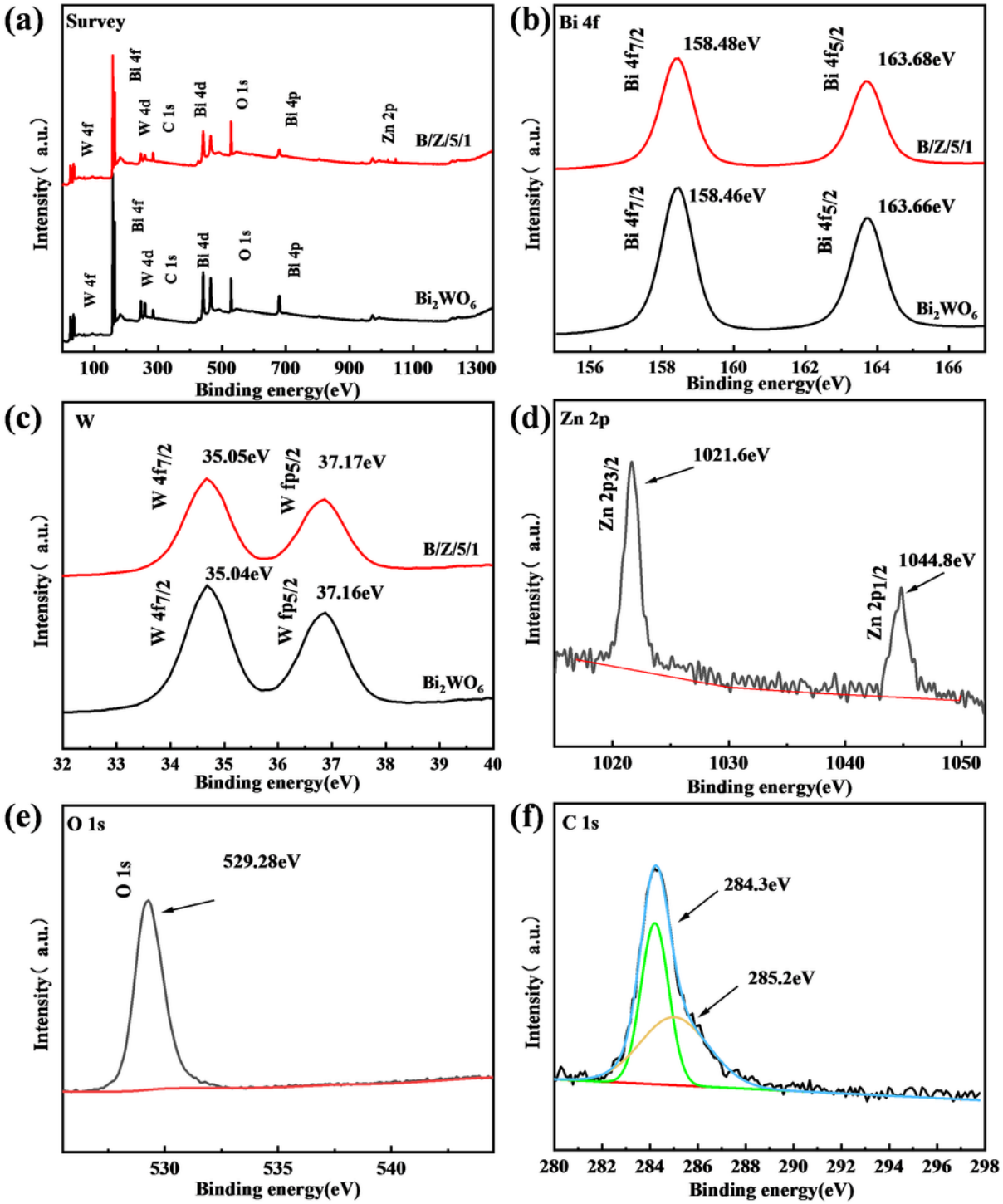

Figure 3

XPS survey spectra of B/Z/5/1 nanocomposites (a), and high resolution XPS spectra of Bi 4f (b), W (c), Zn 2p (d), O 1s (e) and C 1s (f).

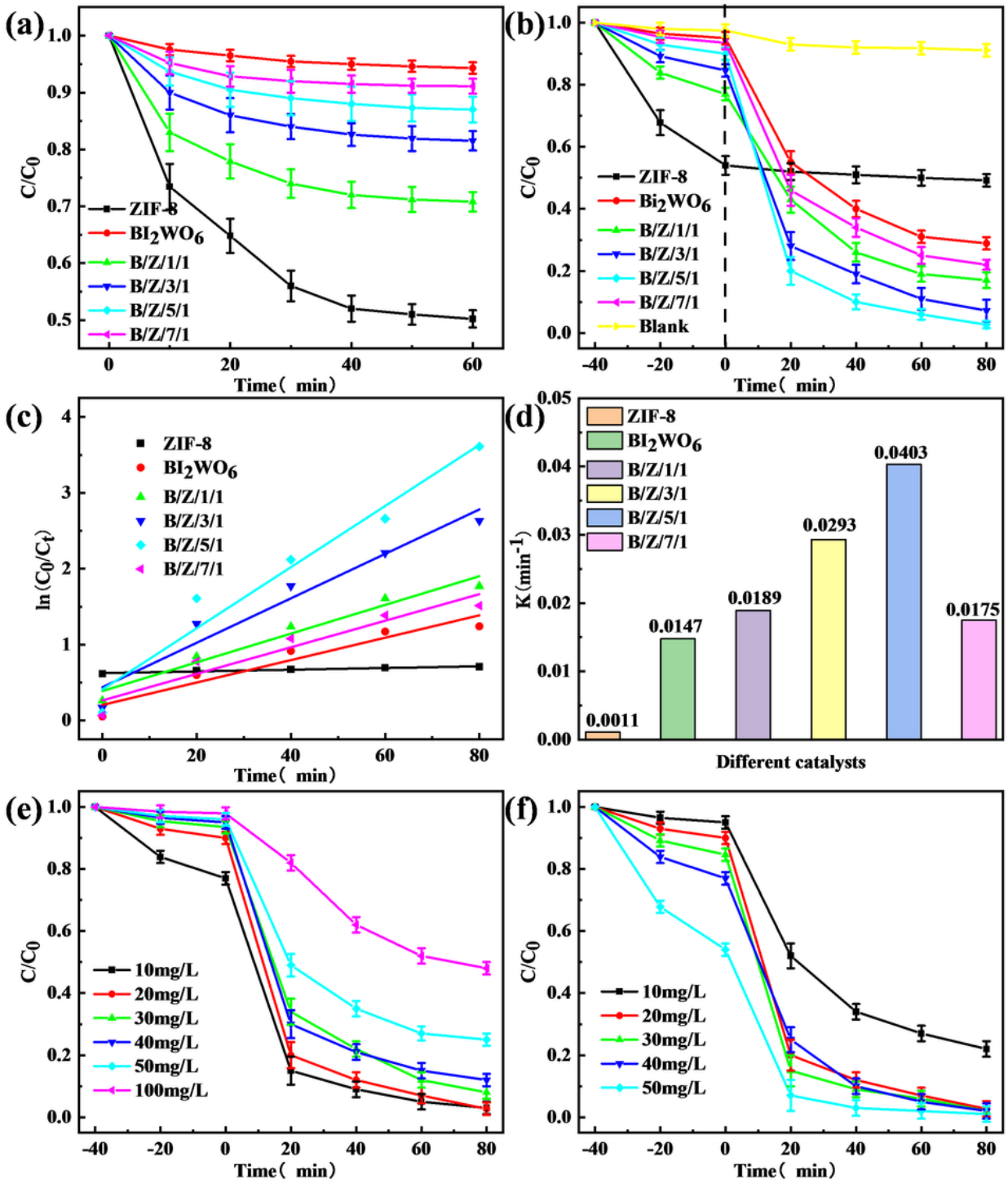

Figure 4

(a) Adsorption properties of different samples for TC; (b) Photocatalytic activity of TC by different samples; (c) Kinetics of photocatalytic degradation of TC by different samples; (d) Effect of different samples on the photocatalytic reaction rate of TC; (e) Degradation of different concentrations of TC; (f) Degradation of TC with different amount of catalyst.

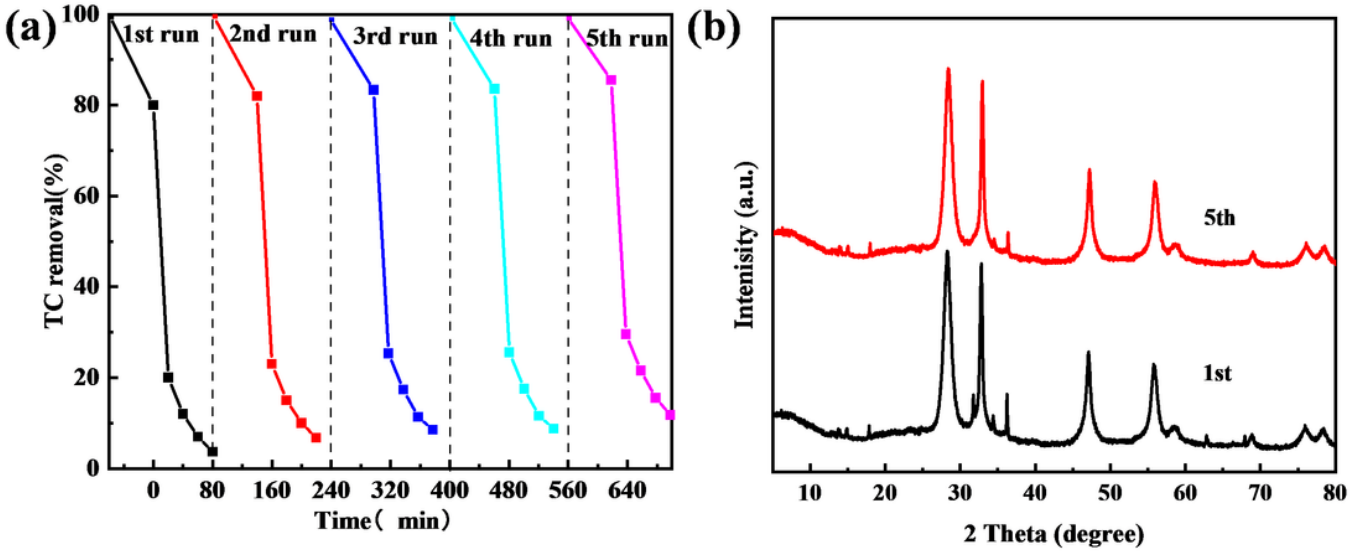

Figure 5

Repeated experiment on degradation of TC by B/Z/5/1 (a) and Comparison of XRD patterns (b)

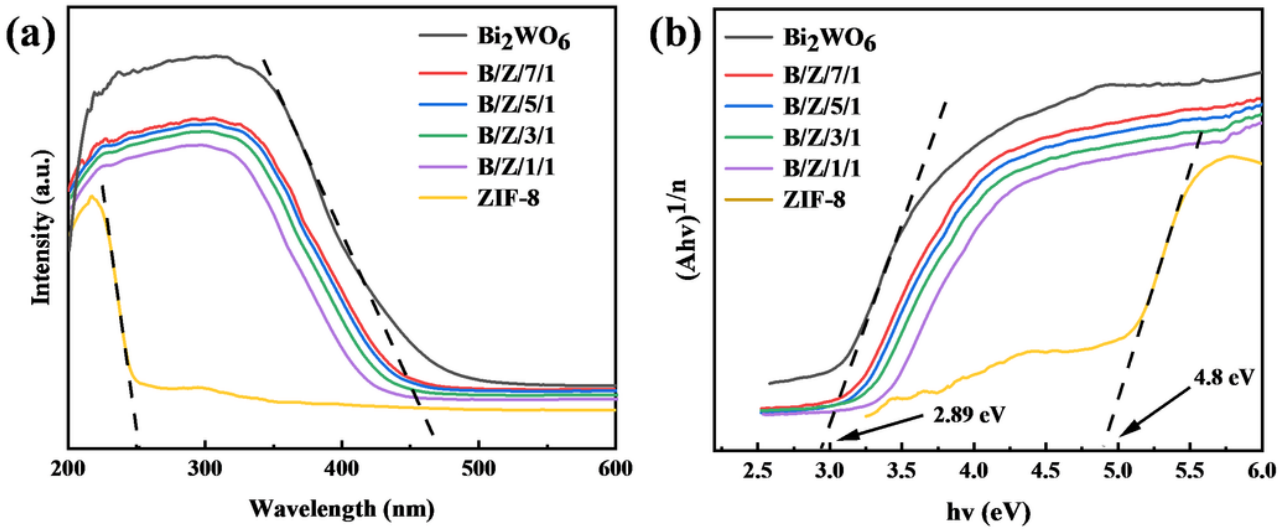

Figure 6

UV–Vis DRS spectra (a) and bandgaps (b) of the samples

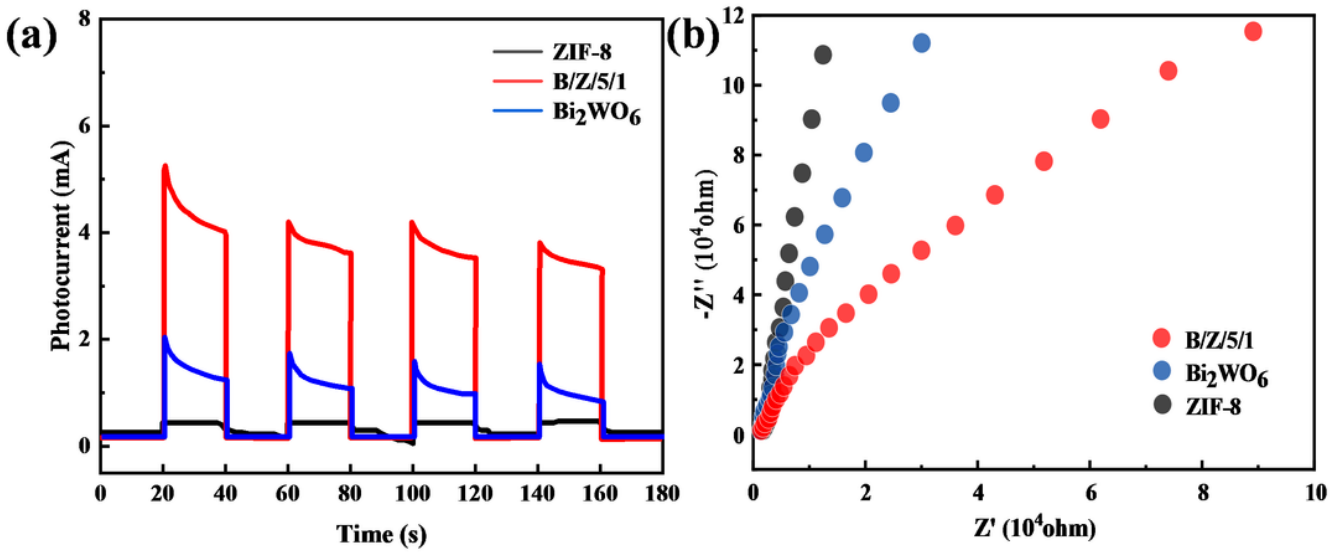

Figure 7

Transient photocurrent response curves (a) and EIS spectra (b) of ZIF-8, Bi2WO6 and B/Z/5/1.

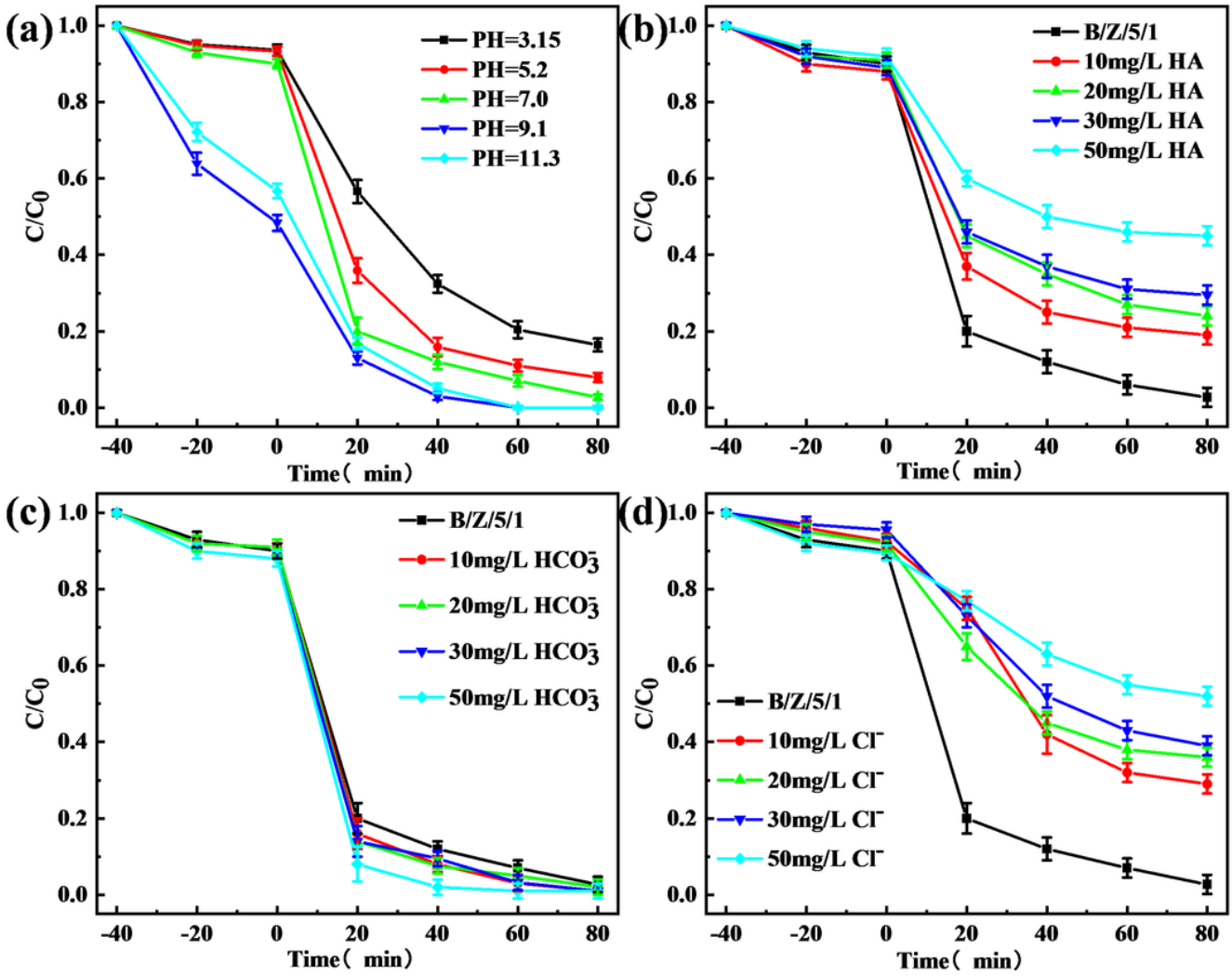

Figure 8

The degradation efficiency of photocatalyst B/Z/5/1 on TC under ultraviolet radiation, different pH (a), different HA concentration (b), different HCO3– concentration (c) and different Cl– concentration (d).

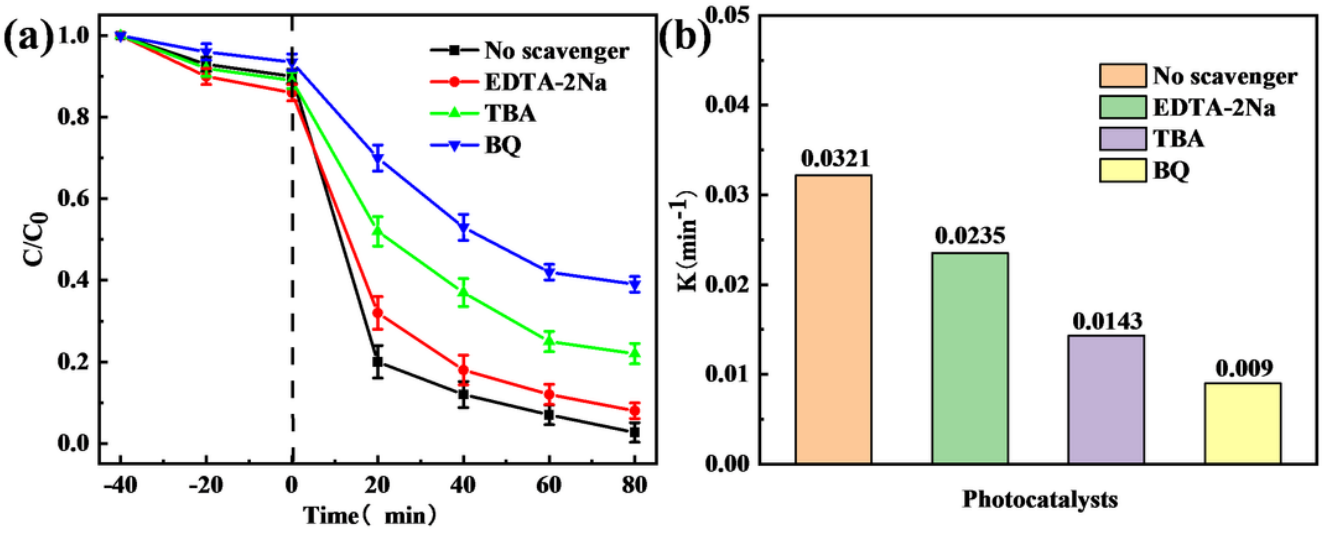

Figure 9

Effects of various trapping agents on photocatalytic efficiency (a), K value of the effect of different trapping agents on B/Z/5/1 (b).

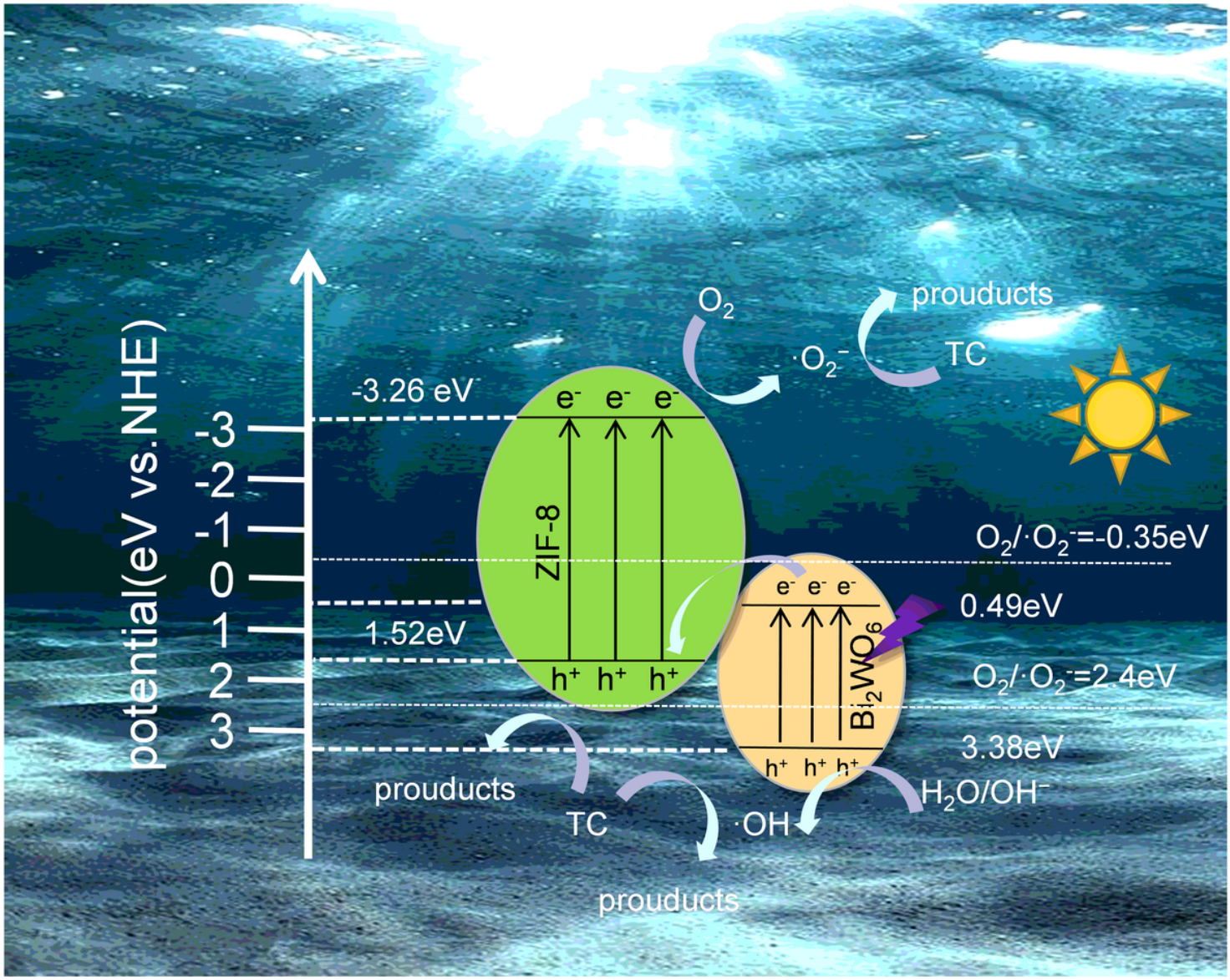

Figure 10

The degradation mechanism of Bi2WO6/ZIF-8 on TC

Supplementary Files

This is a list of supplementary files associated with this preprint. Click to download.

- scheme1.jpg